Applied Physics Letters

A radio-frequency Bose–Einstein condensate magnetometer

Cite as: Appl. Phys. Lett. **120**, 164002 (2022); https://doi.org/10.1063/5.0090776
Submitted: 09 March 2022 • Accepted: 07 April 2022 • Published Online: 21 April 2022
Published open access through an agreement with JISC Collections

Y. Cohen, B. Maddox, C. Deans, et al.

Applied Physics Letters ARTICLE scitation.org/journal/apl

A radio-frequency Bose–Einstein condensate magnetometer

Cite as: Appl. Phys. Lett. **120**, 164002 (2022); doi: 10.1063/5.0090776
Submitted: 9 March 2022 · Accepted: 7 April 2022 ·
Published Online: 21 April 2022

Y. Cohen, B. Maddox, C. Deans,[a] L. Marmugi, and F. Renzoni[b]

AFFILIATIONS

Department of Physics and Astronomy, University College London, Gower Street, London WC1E 6BT, United Kingdom

[a]**Present address:** UKRI National Quantum Computing Centre, Harwell Campus, Didcot OX11 0GD, United Kingdom.
[b]**Author to whom correspondence should be addressed:** f.renzoni@ucl.ac.uk

ABSTRACT

We report on a radio frequency magnetometer employing a Bose–Einstein condensate of ^{87}Rb atoms held in a dipole trap. An AC sensitivity of 296 $\mathrm{pT}/\sqrt{\mathrm{Hz}}$ is achieved at a probing volume of 3.2×10^{-8} cm^3, leading to a volume-normalized sensitivity of 53 $\mathrm{fT}/\sqrt{\mathrm{Hz\,cm^{-3}}}$. At larger probing volumes with the atoms released from the magnetic trap used in the initial phase of the evaporation sequence, the AC sensitivity is improved to 1.4 $\mathrm{pT}/\sqrt{\mathrm{Hz}}$, allowing a two-mode approach for applications requiring improved sensitivity. Immediate application in high-resolution electromagnetic induction imaging is expected when compared to performance of other induction-based imaging platforms.

In recent years, atomic magnetometers have been finding applications in a growing number of techniques, from magnetocardiography[1,2] and magnetoencephalography[3,4] to nuclear magnetic resonance,[5] as they combine extreme sensitivity with reduced size and ease of operation. Extreme sensitivity ($<\mathrm{fT}/\sqrt{\mathrm{Hz}}$) is usually achieved by operating large atomic ensembles near the standard quantum limit, under the form of thermal atomic samples in vapor cells. These setups have the drawback of severely limiting the spatial resolution. This feature makes them unsuitable for high-resolution magnetic field mapping, which has been attracting growing interest. Ideally suited for high-resolution mapping are instead nitrogen-vacancy (NV) diamond magnetometers[6–8] and atomic magnetometers based on ultracold atoms.[9–14] Due to their significantly smaller probing volumes, these high spatial resolution techniques trade-off absolute sensitivity for increased localization. In this work, we demonstrate a radio frequency atomic magnetometer apparatus using a ^{87}Rb Bose–Einstein condensate (BEC) as a sensing medium. By performing magnetometry both within thermal and BEC phases, we study the interplay between sensitivity and probe volume and determine the performance as a function of both quantities. Our results, of direct relevance for magnetic field mapping and high spatial resolution electromagnetic induction imaging (EMI),[15,16] are compared with state-of-the-art magnetometers.

A BEC of ^{87}Rb atoms in the $5^2S_{1/2}|F = 2, m_F = +2\rangle$ state is produced with forced evaporation in a hybrid trap, with the sequence for production illustrated in Fig. 1. Further detail is given in previous communications,[17,18] with a short summary presented here. After loading of the magneto-optical trap (MOT) and a short compression phase (C-MOT), atoms are cooled down to 20 μK via polarization gradient cooling (PGC). Next, optical pumping (OP) into $5^2S_{1/2}|F = 2, m_F = +2\rangle$ allows efficient loading of atoms into the magnetic trap (MT). We note that the spin polarization is maintained during magnetic trapping and subsequent evaporation, and thus, no additional optical pumping is required for the magnetometry phase. The trap is produced by water-cooled quadrupole coils in a PVC mount (40 turns, 4×2 mm^2 cross section copper wire). Initially, the gradient is linearly ramped up to 176 G/cm in 2.5 s, where it is held for a further 5.3 s while an RF (B_{Knife}) field is linearly swept from 13 to 3.5 MHz. Next, the gradient is linearly ramped down to 28 G/cm in 2.25 s and the RF frequency is linearly swept from 3.5 to 0.5 MHz. The now 4 μK atoms can be loaded into the dipole trap dimple in 3 s by lowering the magnetic field gradient linearly to 7 G/cm. The dipole trap consists of two 1064 nm beams (total power 10 W) crossed at an angle of 43.4° and focused down to 80 $\mu\mathrm{m}1/e^2$ radius. The total dipole trap beam power is also exponentially reduced to 0.85 W at this stage (labeled *DT* in Fig. 1) to maximize the phase space density (PSD). The final evaporation consists of exponentially decreasing the total beam power to 0.27 W while linearly increasing the magnetic field gradient to 22 G/cm in 4.7 s.

The BEC is first observed with 6.5×10^4 atoms ($\mathrm{T} < 40$ nK, $\mathrm{PSD} > 1.5$), with increasing condensed fractions as the evaporation continues. An almost pure BEC is seen with 4×10^4 atoms. Measurements of the atom number and PSD are made throughout the sequence.

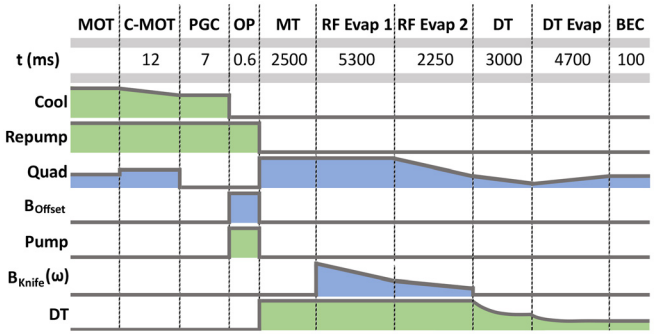

FIG. 1. Sequence for the production of the BEC. Switching of the cooling beams (Cool), repumping beams (Repump), quadrupole field (Quad), offset field for pumping (B_{Offset}), optical pumping beam (Pump), radio frequency field for magnetic trap evaporation (B_{Knife}), and dipole trap beams (DT) is shown. The time for each phase of the sequence is reported, with the duration of the MOT left blank as this can be tailored depending on the required number of atoms (typically 20 s for the experiments reported in this work). Ramping of parameters is shown with either straight lines (linear ramps) or curves (exponential ramps).

Unshielded RF magnetometry is performed in the standard arrangement widely used in vapor cell magnetometry.[19,20] An overview of the setup is shown in Fig. 2. Atoms are held in the dipole trap, spin polarized along $\hat{\mathbf{z}}$, with a bias field applied in the same direction. This induces Zeeman splitting of the atomic levels, with the field produced by circular Helmholtz coils (80 mm diameter). Ambient fields in the $\hat{\mathbf{x}}, \hat{\mathbf{y}}$ directions are passively zeroed by Helmholtz coils (square with side lengths 170, 190 mm, respectively). An RF field, B_{RF}, drives Larmor precession of atomic spins and is produced by a dedicated coil in the $\hat{\mathbf{y}}$ direction (side length 31 mm, 10 turns, 40 mm away from the atoms). This coil is wound around a 3D printed polylactic acid (PLA) mount, which also holds a (Stefan-Mayer FLC100) fluxgate magnetometer near the atomic sample, used for active stabilization of the

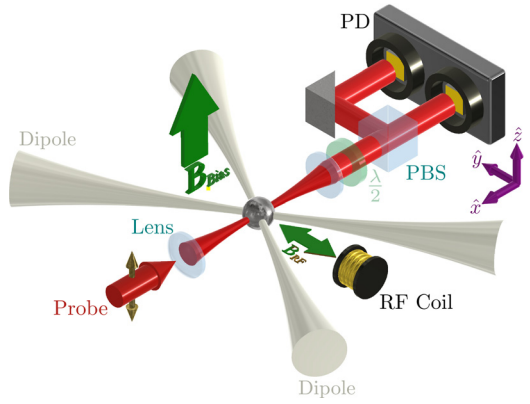

FIG. 2. Setup for ultracold magnetometry, with gravity pointing along $-\hat{\mathbf{z}}$. The BEC is held in the dipole trap (light gray beams). Coils control the magnetic field at the atoms producing both the bias field and the radio frequency field to be measured. Atomic spin precession is monitored with a π polarized probe beam (red). A polarimeter, consisting of a half-wave plate, polarizing beam splitter (PBS), and balanced photodiode (PD) reads out the spin precession. The signal is sampled by a digital oscilloscope. Data are stored by a computer controlled acquisition system, which determines the SNR and linewidth of the magnetic resonance.

bias field. The feedback loop is realized with a proportional-integral-derivative (PID) controller (Stanford Research Systems SIM960) acting on the gate of a MOSFET regulating the current supplied to the coils. A solid-state relay ensures the stabilization only occurs during the magnetometry phase, with large gradients during magnetic trapping forbidding continuous stabilization during the cold atoms sequence due to sensor saturation. Active stabilization of the bias field sees a x2 improvement in sensitivity, similar to previously quoted results in unshielded vapor cell magnetometers.[21]

Atomic spin precession is probed via Faraday rotation of a π polarized beam, propagating along the $\hat{\mathbf{x}}$ direction and detuned by $+330$ MHz from the ^{87}Rb $5^2S_{1/2}, F = 2 \rightarrow 5^2P_{3/2}, F' = 3$ cooling transition. For all measurements presented in this work, the probe interacts with the atoms for 4 ms. The probe beam is extracted from cooling light, passing through a double pass acousto-optic modulator (AOM) setup to achieve increased detuning from the cooling transition and a single pass AOM for intensity stabilization behind a high-speed mechanical shutter. The probe is then focused down to a $1/e^2$ diameter of 126 μm at the atoms for BEC magnetometry with a mean intensity of 366 mW cm^{-2}. The probe polarization is monitored via a polarimeter, consisting of a polarizing beam splitter (PBS) and a balanced photodiode (PD) (Thorlabs PDB210A). The polarimeter signal is sampled by a digital oscilloscope (PicoScope 4262). A Keysight 33120A Signal Generator is used to send a triggered burst to the RF coil. Data are acquired by a LabVIEW program, which computes the fast Fourier transform (FFT) of the oscilloscope sampled signal to extract the signal to noise ratio (SNR). To determine the resonance shape and width, lock-in amplification is performed on polarimeter signals acquired at different frequencies with MATLAB.

Figure 3(a) shows an amplitude spectrum for 6.3×10^4 atoms in the BEC held in the dipole trap with a probe volume of 3.2×10^{-8} cm^3. The bias field (B_{Bias}) is set to 17.3 μT (121.5 kHz), and a calibration field (B_{RF}) of magnitude 34 nT is applied. The total noise defines the SNR as 7, leading to an AC sensitivity of $\delta B_{AC}^{BEC} = 296\,\mathrm{pT}/\sqrt{\mathrm{Hz}}$ in our measurement time of 4 ms. Sweeping the calibration field frequency results in an in-phase Lorentzian profile and out of phase dispersive profile referenced to the driving field, illustrated in Fig. 3(b). This allows extraction of the half-width at half-maximum (HWHM) of the resonance (Γ), calculated to be 1.1 kHz from the fit of the dispersive, leading to a DC sensitivity of $\delta B_{DC}^{BEC} = 225\,\mathrm{pT}/\sqrt{\mathrm{Hz}}$.

Next, the scaling of the magnetometer's sensitivity with atom number and volume is investigated. Both are changed by controlling the dipole trap's intensity at the end of the evaporation while maintaining the evaporation duration. This is illustrated in Fig. 4, where the phase transition is highlighted by the difference in color of the data points. A fit to the data suggests the sensitivity scales as $\propto N^{-1.3}$, which is in agreement (within confidence intervals) to previously reported data for cold atoms.[18] This confirms the BEC magnetometer is not spin-projection noise limited. Importantly, we do not see a change in the scaling across the phase transition. A similar scaling can be extracted for the dependency of the sensitivity on volume, which is found to scale as $\propto V^{-0.95}$.

We now introduce a different measurement mode, where atoms are probed after being released from the magnetic trapping potential. A much larger atom number of 3×10^8 atoms at a probing volume of 0.14 cm^3 achieves improved sensitivity at the cost of an increase in

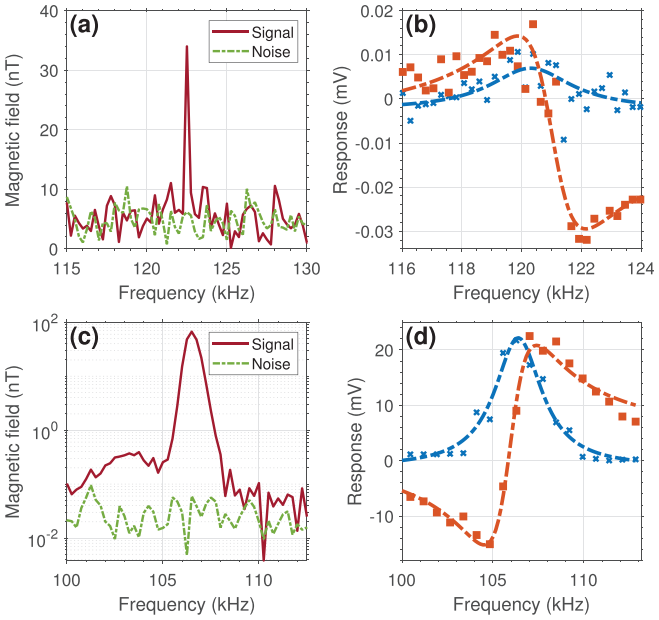

FIG. 3. Typical response of the magnetometer, both with the BEC held in the dipole trap potential (a) and (b) (6×10^4 atoms) and with atoms after release from the magnetic trap phase (c) and (d) (3×10^8 atoms). Parts (a) and (c) show an amplitude spectrum from the FFT of the polarimeter signal scaled to the calibration field magnitude with both the noise (light green) and signal (red) plotted. Parts (b) and (d) show the phase sensitive detection of the magnetic resonance used to determine the linewidth. The shape of the dispersive is inverted in the two measurement modes due to opposite bias field directions.

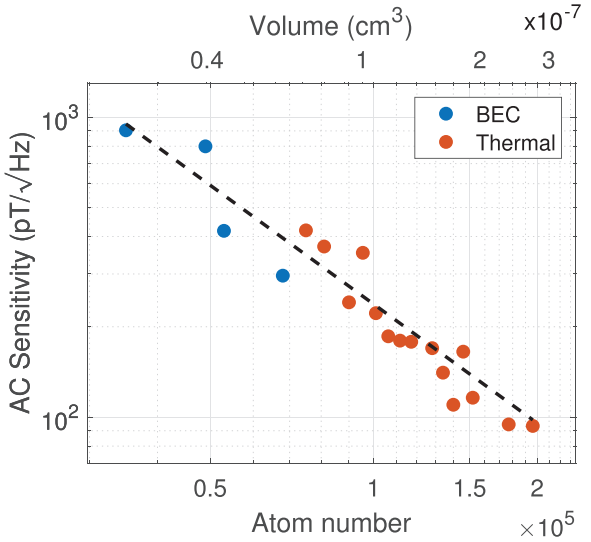

FIG. 4. Scaling of AC sensitivity with atom number and volume. The dipole trap intensity at the end of the evaporation is varied while maintaining the total evaporation duration. Atom number, volume, and sensitivity are all measured. As the atom number and volume reduces, a phase transition occurs, which is highlighted by different color of data points.

probing volume. For magnetometry in this regime, the beam has a $1/e^2$ diameter of 4 mm, matching the size of the atomic cloud, with a mean intensity of 568 μW/cm^2. Figure 3(c) shows an amplitude spectrum in this magnetometry regime with the bias field (B_{Bias}) set to 15.2 μT (106.5 kHz) and an applied calibration field (B_{RF}) of magnitude 63 nT. The total noise (same conditions, calibration field off) defines the SNR as 2632, leading to an AC sensitivity of Ref. 19 $\delta B_{AC}^{MT} = 1.6\,\mathrm{pT}/\sqrt{\mathrm{Hz}}$. Part (d) shows a typical phase sensitive response. Γ is extracted from the fit of the dispersive as 1.27 kHz, leading to a value for the DC sensitivity close to the one derived for the AC sensitivity, $\delta B_{DC}^{MT} = 1.4\,\mathrm{pT}/\sqrt{\mathrm{Hz}}$.

It is interesting to compare the presented results with the state-of-the-art of EMI. The BEC RF-AM is very promising both in terms of frequency tunability and volume-normalized sensitivity. At minimum probe volume in the BEC, the volume-normalized sensitivity is calculated to be $53\,\mathrm{fT}/\sqrt{\mathrm{Hz\,cm^{-3}}}$. Compared to EMI systems utilizing vapor cell atomic magnetometers, the BEC RF-AM has a similar volume-normalized sensitivity.[21] However, these use large atomic ensembles with a minimum probe volume, which is six orders of magnitude larger than that in the BEC RF-AM, rendering such systems unsuitable for high spatial resolution EMI. When compared to recent works using an NV-diamond magnetometer that demonstrated high-spatial resolution EMI,[22] the BEC RF-AM improves on the volume-normalized sensitivity by a factor of two.

In conclusion, we have reported on an ultracold radio frequency magnetometer with volume-normalized sensitivity suitable for high spatial resolution magnetic field mapping. By considering the trade-off of sensitivity and probing volume, such a BEC-based device could have a two-mode approach when improved sensitivity is required at lower spatial resolution (or the opposite). This is not possible in many of the previously reported high spatial resolution sensors. Seven orders of magnitude in probing volume are demonstrated, down to 2.3×10^{-8} cm^3, with a minimum AC sensitivity of $1.4\,\mathrm{pT}/\sqrt{\mathrm{Hz}}$. In terms of absolute performance, at minimum probe volume in the BEC, the volume-normalized sensitivity is calculated to be $53\,\mathrm{fT}/\sqrt{\mathrm{Hz\,cm^{-3}}}$. This confirms that EMI with a BEC is possible in our system, allowing us to explore the prospect of electromagnetic induction microscopy and its applications in nanotechnology. This can be realized by moving the BEC close to the walls of the vacuum chamber and placing the object in close proximity to the external wall. EMI can then be performed by taking measurements for different displacements of the object with respect to the BEC.

The authors thank Sindi Sula for contributions to the early phase of the experiment. This work was funded by the Engineering and Physical Sciences Research Council (EPSRC) Impact Acceleration Account (Grant No. EP/R511638/1).

AUTHOR DECLARATIONS

Conflict of Interest

The authors have no conflicts to disclose.

DATA AVAILABILITY

The data that support the findings of this study are available from the corresponding author upon reasonable request.

REFERENCES

[1]J. Belfi, G. Bevilacqua, V. Biancalana, S. Cartaleva, Y. Dancheva, and L. Moi, J. Opt. Soc. Am. B **24**, 2357 (2007).
[2]R. Wyllie, M. Kauer, R. T. Wakai, and T. G. Walker, Opt. Lett. **37**, 2247 (2012).
[3]H. Xia, A. Ben-Amar Baranga, D. Hoffman, and M. V. Romalis, Appl. Phys. Lett. **89**, 211104 (2006).
[4]V. K. Shah and R. T. Wakai, Phys. Med. Biol. **58**, 8153 (2013).
[5]I. M. Savukov and M. V. Romalis, Phys. Rev. Lett. **94**, 123001 (2005).
[6]L. Rondin, J.-P. Tetienne, T. Hingant, J.-F. Roch, P. Maletinsky, and V. Jacques, Rep. Prog. Phys. **77**, 056503 (2014).
[7]A. Wickenbrock, H. Zheng, L. Bougas, N. Leefer, S. Afach, A. Jarmola, V. M. Acosta, and D. Budker, Appl. Phys. Lett. **109**, 053505 (2016).
[8]G. Chatzidrosos, A. Wickenbrock, L. Bougas, H. Zheng, O. Tretiak, Y. Yang, and D. Budker, Phys. Rev. Appl. **11**, 014060 (2019).
[9]M. Vengalattore, J. M. Higbie, S. R. Leslie, J. Guzman, L. E. Sadler, and D. M. Stamper-Kurn, Phys. Rev. Lett. **98**, 200801 (2007).
[10]S. Wildermuth, S. Hofferberth, I. Lesanovsky, S. Groth, P. Krüger, J. Schmiedmayer, and I. Bar-Joseph, Appl. Phys. Lett. **88**, 264103 (2006).
[11]R. J. Sewell, M. Koschorreck, M. Napolitano, B. Dubost, N. Behbood, and M. W. Mitchell, Phys. Rev. Lett. **109**, 253605 (2012).
[12]O. Elíasson, R. Heck, J. S. Laustsen, M. Napolitano, R. Müller, M. G. Bason, J. J. Arlt, and J. F. Sherson, J. Phys. B **52**, 075003 (2019).
[13]N. Sekiguchi, K. Shibata, A. Torii, H. Toda, R. Kuramoto, D. Fukuda, and T. Hirano, Phys. Rev. A **104**, L041306 (2021).
[14]S. Palacios Alvarez, P. Gomez, S. Coop, R. Zamora-Zamora, C. Mazzinghi, and M. W. Mitchell, Proc. Natl. Acad. Sci. **119**, e2115339119 (2022).
[15]H. Griffiths, Meas. Sci. Technol. **12**, 1126 (2001).
[16]C. Deans, L. Marmugi, S. Hussain, and F. Renzoni, Appl. Phys. Lett. **108**, 103503 (2016).
[17]R. Nolli, M. Venturelli, L. Marmugi, A. Wickenbrock, and F. Renzoni, Rev. Sci. Instrum. **87**, 083102 (2016).
[18]Y. Cohen, K. Jadeja, S. Sula, M. Venturelli, C. Deans, L. Marmugi, and F. Renzoni, Appl. Phys. Lett. **114**, 073505 (2019).
[19]I. M. Savukov, S. J. Seltzer, M. V. Romalis, and K. L. Sauer, Phys. Rev. Lett. **95**, 063004 (2005).
[20]D. Budker and M. Romalis, Nat. Phys. **3**, 227 (2007).
[21]C. Deans, L. Marmugi, and F. Renzoni, Rev. Sci. Instrum. **89**, 083111 (2018).
[22]C. Xu, J. Zhang, H. Yuan, G. Bian, P. Fan, M. Li, and T. Liu, Appl. Phys. Lett. **120**, 084104 (2022).